

An Underactuated Multi-finger Grasping Device

Regular Paper

Cesare Rossi^{1,*} and Sergio Savino²

¹ University of Naples - Naples, Italy

² D.I.I. University of Naples "Federico II", Italy

* Corresponding author E-mail: cesare.rossi@unina.it

Received 15 Oct 2013; Accepted 16 Nov 2013

DOI: 10.5772/57419

© 2014 The Author(s). Licensee InTech. This is an open access article distributed under the terms of the Creative Commons Attribution License (<http://creativecommons.org/licenses/by/3.0>), which permits unrestricted use, distribution, and reproduction in any medium, provided the original work is properly cited.

Abstract In this paper, a mechanical model for an underactuated multi-finger grasping device is presented. The device has single-tendon, three-phalanx fingers, all moved by only one actuator. By means of the model, both the kinematic and dynamical behaviour of the finger itself can be studied. The finger is part of a more complex mechanical system that consists of a four-finger grasping device for robots or a five-finger human hand prosthesis. Some results of both the kinematic and dynamical behaviour are also presented.

Keywords Mechanical Finger, Robotic Hand, Gripper

1. Introduction

In the last decades, many devices for human prostheses have been developed; moreover, several devices for grasping end effectors for robots, based on a human hand design, have also been developed. These devices have greatly contributed to the handling capabilities of robots and, even more importantly, improved the quality of life of a considerable number of people.

It is well-known that the human hand is one of the most complex and multi-functional organs; even ignoring the

thumb's capability to rotate, the hand still has 15 d.o.f. Obviously, the great progress in actuator miniaturization and in control systems make it possible to design multi-finger and multi-phalanx grasping tools operated by several actuators; nevertheless, both the mechanical parts and the control mechanisms are very complex, hence the cost is very high while the reliability is rather low.

For the reasons mentioned above, an underactuated multi-finger grasping device with three phalanxes fingers moved by a single actuator would be of considerable interest.

Several multi-finger systems that work like the human hand or even consist of human prostheses have been developed. It must be said that, despite the progress in micro motors, in the grasping devices that use fingers, if the system's dimensions are comparable to those of a human hand, it is rather difficult to operate each of the finger phalanxes with a (micro)motor, so the fingers are moved by tendons.

In Figure 1 some examples are shown. In Figure 1,a a schematic [1] of a five-finger hand moved by a single actuator is shown; the auto-adaptability of the fingers to the shape of the grasped object is obtained by means of "sliding pulleys". In Figure 1b a study [2] is presented, in

which a synergy concept was developed, based on the anatomic links of the human hand between the muscle and the tendons mostly as far as the coordination of the fingers is concerned (eigenpostures); this was obtained, essentially, by means of a number of pulleys fitted on the same shaft but with different diameters, as shown in Figure 1,c. It must be said that the early prototypes did not achieve the desired finger positions very accurately; the behaviour of the device was then improved by increasing the mechanical and control complexity, using a further actuator and a gear system.

In Figure 1,d a model [3] widely inspired by the human body is shown; most of the phalanxes' joints are of variable stiffness, allowing for greater exertion and better adaptability. Since the hand is designed to be part of a mechanical arm, the motors are located in the arm. The fingers are operated in an antagonistic way by two motors for each d.o.f. and 38 motors, fitted in the forearm, were used; hence the device is not underactuated.

In Figure 1,e a first prototype (see e.g., [4]) developed at the Scuola Superiore Sant'Anna (Pisa, Italy) is shown, which has 16 d.o.f., operated by four motors, which was further developed in subsequent research activities (see e.g., [5-8]). Another Italian research team, borne from the collaboration between the University of Pisa and the Research Center "E.Piaggio", rather recently, developed the hand shown in Figure 1,f, (see e.g., [9]). The device is operated by one actuator only, the joints are based on the Hillberry joint and the tendons are elastic.

In Figure 1,g the Multifunctional Hand Prosthesis is shown [10]. Eight fluid operated actuators are used, fed by a pump fitted in the metacarpal together with micro-valves controlled by a micro-controller.

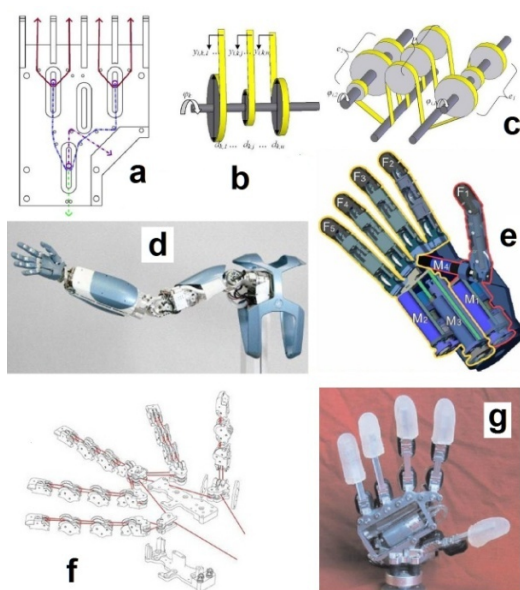


Figure 1. Examples of hand models and mechanisms, [1-4, 9,10]

In Figure 2,a and b the "Larm hand" is shown as is the kinematic schematic for one finger of a grasping device developed at the University of Cassino (Italy) [11,12,13,14], that essentially consists of a four-finger underactuated hand.

In Figure 2,c the Southampton Remedi Hand [15] is shown; it has six d.o.f. with six small motors; four of them move the fingers and two move the thumb.

The above-mentioned developments and further developments in the investigations into underactuated devices presented in [16] are perhaps among the most representative examples of mechanical hands. As for the underactuated designs, it can be said that there are essentially two types, schematically shown in Figure 2,d. The soft synergy is essentially based on the presence of elastic tendons while adaptive synergies are essentially based on differential mechanisms. During the grasping motion, both the systems permit the fingers to adapt themselves to objects of a complicated shape (i.e., different sections in correspondence with each of the fingers), but the adaptive synergies with "rigid" tendons enable, also, the hand to grip the object and exert practically the same gripping force.

As for the tendon operated fingers, different solutions can be adopted, as was reported in [17]; possible solutions range from a tendon for each of the phalanxes to a single tendon for the three phalanxes; the joints between the latter can be represented by simple hinges or more complex kinematic systems or even by simple elastic links.

Given the above, studying the possibility of designing a rather simple and cheap hand, based on adaptive synergies underactuated by means of a single actuator would be of considerable interest.

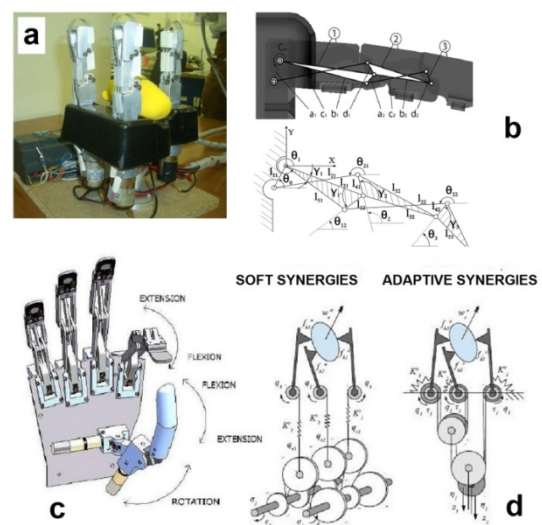


Figure 2. Examples of hand models and mechanisms, [11-16]

2. Aim of the study

As mentioned previously, the aim of this study is to evaluate the possibility of designing a rather simple and cheap hand, based on adaptive synergies underactuated by means of a single actuator. The study will be carried out by proposing both kinematic and dynamic models for the mechanism and evaluating their behaviour by means of computer simulation codes.

Finally, some possible further improvements are also discussed.

3. Description of the mechanisms

Both the grasping device for robots and the five-finger human hand prosthesis are based on an adaptive scheme similar to those shown in Figures 1,a and 2,d. This solution was essentially adopted for the following reasons:

- An underactuated system seemed to be the simplest, least expensive and lightest in weight.
- An adaptive synergy with rigid tendons allow the hand to grip the object and exert practically the same gripping force.
- The described solution can be easily improved in order to obtain a smarter control of each of the fingers.

In Figure 3, a pulley-based adaptive system is shown. If, X_s , X_D and X_P are the displacements of the centres of the pulleys, respectively left, right and main, θ_s , θ_D and θ_P are the respective rotations and X_1 , X_2 , X_3 and X_4 are the displacements of the ends of the tendons.

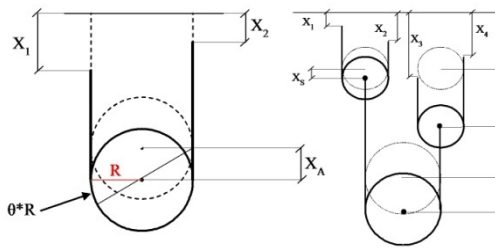


Figure 3. Pulleys system

The following relations can be easily written:
For a single pulley:

$$x_1 = x_A + \vartheta \cdot R \quad (1)$$

$$x_2 = x_A - \vartheta \cdot R \quad (2)$$

$$\vartheta = \frac{x_1 - x_A}{R} \quad (3)$$

And for the multi-pulley system:

$$X_A = \frac{x_1 + x_2}{2} \quad (4)$$

$$X_S = \frac{x_1 + x_2}{2} \quad (5)$$

$$X_D = \frac{x_3 + x_4}{2} \quad (6)$$

$$X_P = \frac{x_1 + x_2 + x_3 + x_4}{4} \quad (7)$$

If the four displacements are equal, none of the three pulleys will rotate, while, if they are different, the pulleys will rotate to a suitable angle to ensure the desired configuration.

In Figure 4, the schema of three possible configurations for a four-finger system are shown; in the configuration on the right, the thumb can be either movable or fixed. In the Figure, the structure of the finger is also shown.

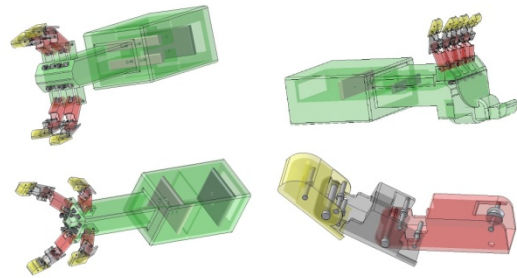


Figure 4. Cad models of hands and finger prototypes

In Figure 5, a prototype for a hand prosthesis is shown, based on the same adaptive system.

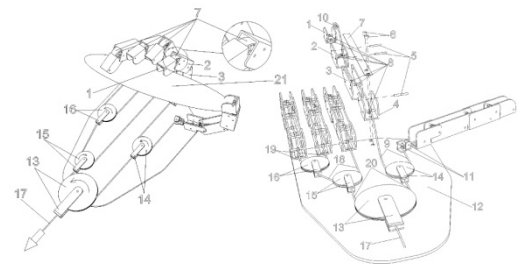


Figure 5. Prototype of a hand prosthesis

In Figure 6, a simulation by Working Model 2D™ is shown.

The Figure shows the following: on the left the mechanism with open fingers, on the left an object held by the fingers, and A indicates a generic section of the object. The latter is modelled by a fixed circle and a solid square linked to the circle by means of a rod; this is in

order to simulate an object, the section of which can change during the grasping. In the model, the pulleys were modelled by means of a rocker. On the left side of the Figure, it is possible to observe that in correspondence to each of the fingers, the size of the solid circle is different; this is in order to simulate an object with variable sections. It is also possible to observe that the position of the squares is changed, simulating an object changing shape during the grasping. The kinematic simulation results clearly show that the mechanism allows the fingers to correctly grasp any of the object's sections; this is because of the pulleys' (rocker) rotation and because of the correct positioning of the tendons' guides.

This latter aspect will be shown in the following paragraph.

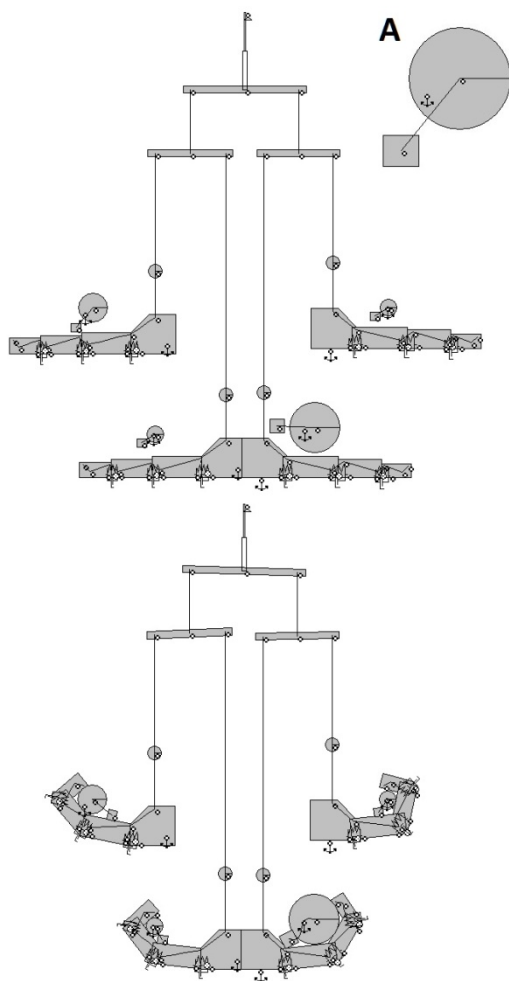


Figure 6. Working Model simulation

By using Working Model 2D™ it is also possible to determine the inertial forces on the phalanxes during the approach to the object: one example is reported in Figure 7.

From the Figure it is possible to observe that the maximum force exerted by any of the phalanxes ranges between 1 N and 2 N independently of the position it assumes at the grasping. This suggests that the maximum force that will

stress the object can also be easily controlled by simply regulating the force exerted by the actuator.

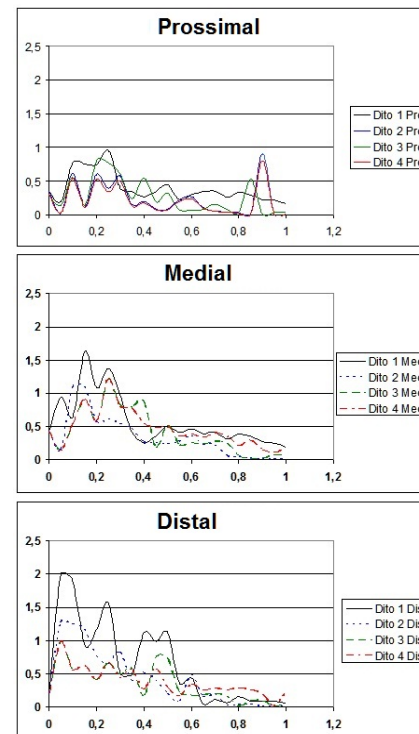


Figure 7. Working Model simulation results

4. The finger

The finger was already shown in Figure 4. In order to study its behaviour, a simplified diagram of it was considered; it is shown in Figure 8.

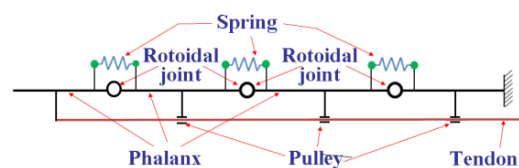


Figure 8. Simplified diagram of the finger

The mechanism, thus conceived, is a system with a single degree of freedom and with two degrees underactuated. In Table 1 the main characteristic data of the kinematic chain are shown which must be studied.

Number of links	4
Number of hinges	3
Number of tendons	1
Number of pulleys	4
Number of springs	3
Number of actuators.	1
Degree of freedom	1
Underactuated degree	2

Table 1. Finger characteristic data

4.1 Kinematic study

This paragraph shows the kinematics of the model of the developed finger.

The operating principle of the mechanism is very simple. Since the finger is an underactuated system, it consists of three joints of which one is active and two are passive, its different possible configurations are related to shortening the one tendon that is moved by the one actuator that constitutes it.

The pulling force that the actuator gives the tendon acts on the mechanism through the point of attack on the distal phalanx and through the set of pulleys. Shortening the tendon by a certain amount, the three phalanges will rotate an amplitude that will be different depending on the value of the stiffness of the elastic elements. For the purposes of the study of the kinematics of the articulated finger, we can say that for each configuration assumed, the total shortening will be the sum of three aliquots, each linked to the rotation of the individual phalanges.

4.1.1 Tendon and elastic elements modelling

In Figure 9 a generic phalanx (i) is shown schematically, for which the following points have been identified:

$C_i(X_{c_i}, Y_{c_i}, Z_{c_i})$ = hinge with the previous phalanx in reference (X_i, Y_i, Z_i) ;

$C_{i+1}(X_{c_{i+1}}, Y_{c_{i+1}}, Z_{c_{i+1}})$ = hinge with the subsequent phalanx in reference (X_i, Y_i, Z_i) ;

$M'_i(X_{M'_i}, Y_{M'_i}, Z_{M'_i})$ = coupling point of the elastic element i with the previous phalanx in reference (X_i, Y_i, Z_i) ;

$M''_i(X_{M''_i}, Y_{M''_i}, Z_{M''_i})$ = coupling point of the elastic element i with the subsequent phalanx in reference $(X_{i+1}, Y_{i+1}, Z_{i+1})$;

$V_i(X_{V_i}, Y_{V_i}, Z_{V_i})$ = coupling point of the pulley on which the tendon slides in reference (X_i, Y_i, Z_i) .

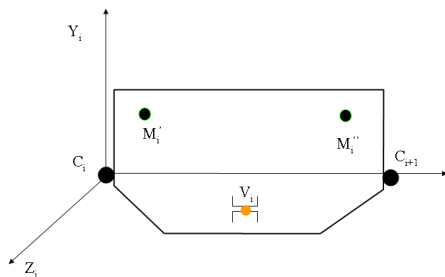


Figure 9. Simplified diagram of a generic phalanx

Given two contiguous phalanges (i-1), (i) it is possible to determine the triangle formed by (C_i) , (V_i) and (V_{i-1}) , as shown in Figure 10. Since the points (V_i) and (V_{i-1}) are fixed

with respect to (C_i) , in the triangle formed by them, the lengths of the two sides, $(V_i C_i)$ and $(V_{i-1} C_i)$, are constant for any configuration, while the third side, identified from the tendon, varies with the rotation of the phalanx (i).

From the diagram in Figure 10, it is possible to obtain the following geometric relationships:

$$rt_i = \sqrt{x_{v_i}^2 + y_{v_i}^2} \quad (8)$$

$$dt_{i-1} = \sqrt{(x_{c_i} - x_{v_{i-1}})^2 + (y_{c_i} - y_{v_{i-1}})^2} \quad (9)$$

If θ_i is the angle of the rotation of the phalanx (i), and if it is determined that this can only rotate in a clockwise direction and it is supposed that the hinges and the pulleys are aligned between them, it is possible to define the quantities that are indicated in Figures 10 and 11.

When $\theta_i=0$:

$$\alpha_{(i-1)_0} = a \tan 2 \left(\frac{(y_{c_i} - y_{v_{i-1}})}{(x_{c_i} - x_{v_{i-1}})} \right) \quad (10)$$

$$\gamma_{(i)_0} = a \tan 2 \left(\frac{|y_{v_i}|}{x_{v_i}} \right) \quad (11)$$

$$\beta_{(i)_0} = \pi - \alpha_{(i-1)_0} - \gamma_{(i)_0} \quad (12)$$

$$lt_{(i)_0} = \sqrt{dt_{i-1}^2 + rt_i^2 - 2dt_{i-1} \cdot rt_i \cos \beta_{(i)_0}} \quad (13)$$

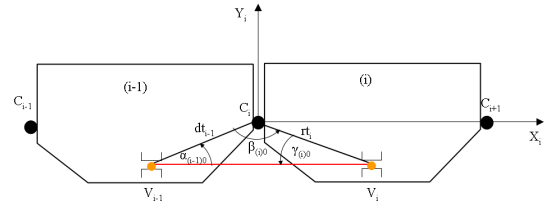


Figure 10. Tendon diagram for two contiguous phalanges with $\theta_i=0$

When $\theta_i > 0$, the reference scheme is that of Figure 11 and it is possible to derive the following relations:

$$\alpha_{(i-1)\theta} = a \cos \left(\frac{lt_{(i)\theta}^2 + dt_{(i-1)}^2 - rt_{(i)}^2}{2 \cdot lt_{(i)\theta} \cdot dt_{(i-1)}} \right) \quad (14)$$

$$\gamma_{(i)\theta} = a \cos \left(\frac{lt_{(i)\theta}^2 + rt_{(i)}^2 - dt_{(i)}^2}{2 \cdot lt_{(i)\theta} \cdot rt_{(i)}} \right) \quad (15)$$

$$\beta_{(i)\theta} = \beta_{(i)_0} - \theta_i = \pi - \alpha_{(i-1)_0} - \gamma_{(i)_0} - \theta_i \quad (16)$$

$$lt_{(i)\theta} = \sqrt{dt_{i-1}^2 + rt_i^2 - 2dt_{i-1} \cdot rt_i \cos \beta_{(i)\theta}} \quad (17)$$

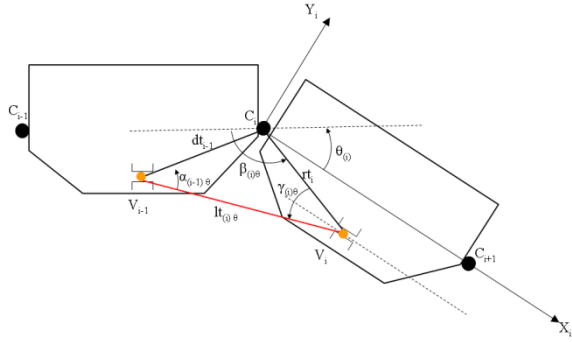


Figure 11. Tendon diagram for two contiguous phalanges with $\theta_i > 0$

The difference between the length of the tendon in the undeformed configuration, $l_{t(i)0}$, and the same in the deformed configuration, $l_{t(i)\theta}$, constitutes the "local" shortening of the entire tendon $\Delta l_{t(i)\theta}$.

$$\Delta l_{t(i)\theta} = l_{t(i)0} - l_{t(i)\theta} \quad (18)$$

The calculation can be repeated for all the phalanges of the articulated mechanism, thus evaluating the "local" shortenings of the tendon due to rotations around each of the three hinges, the sum of which constitutes the total shortening of the tendon in the deformed configuration of the kinematic chain.

If n is the number of hinges, and so of phalanges, the total shortening of the tendon is:

$$\Delta l_{t(Tot)\theta} = \sum_{i=1}^n \Delta l_{t(i)\theta} \quad (19)$$

As for the elastic elements, similar considerations can be made as those for the tendon. From the diagram of Figure 12, it is possible to obtain the following geometric relationships:

$$rm_{(i)} = \sqrt{x_{M'_i}^2 + y_{M'_i}^2} \quad (20)$$

$$dm_{(i)} = \sqrt{x_{M'_{i-1}}^2 + y_{M'_{i-1}}^2} \quad (21)$$

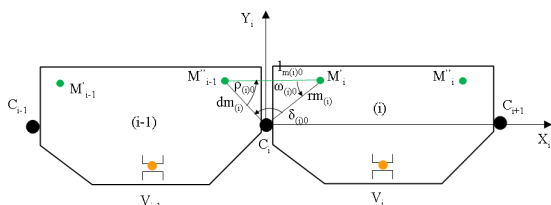


Figure 12. Elastic element diagram for two contiguous phalanges with $\theta_i = 0$

When $\theta_i = 0$:

$$\rho_{(i)0} = a \tan 2 \left(\frac{y_{M'_{i-1}}}{x_{M'_{i-1}}} \right) \quad (22)$$

$$\omega_{(i)0} = a \tan 2 \left(\frac{y_{M'_i}}{x_{M'_i}} \right) \quad (23)$$

$$\delta_{(i)0} = \pi - \rho_{(i)0} - \omega_{(i)0} \quad (24)$$

$$lm_{(i)0} = \sqrt{dm_{(i)}^2 + rm_{(i)}^2 - 2dm_{(i)} \cdot rm_{(i)} \cos \delta_{(i)0}} \quad (25)$$

When $\theta_i > 0$, the reference scheme is that of Figure 13 and it is possible to derive the following relations:

$$\rho_{(i)\theta} = a \cos \left(\frac{lm_{(i)\theta}^2 + dm_{(i)}^2 - rm_{(i)}^2}{2 \cdot lm_{(i)\theta} \cdot dm_{(i)}} \right) \quad (26)$$

$$\omega_{(i)\theta} = a \cos \left(\frac{lm_{(i)\theta}^2 + rm_{(i)}^2 - dm_{(i)}^2}{2 \cdot lm_{(i)\theta} \cdot rm_{(i)}} \right) \quad (27)$$

$$\delta_{(i)\theta} = \delta_{(i)0} + \theta_i = \pi - \rho_{(i)\theta} - \omega_{(i)\theta} + \theta_i \quad (28)$$

$$lm_{(i)\theta} = \sqrt{dm_{(i)}^2 + rm_{(i)}^2 - 2dm_{(i)} \cdot rm_{(i)} \cos \delta_{(i)\theta}} \quad (29)$$

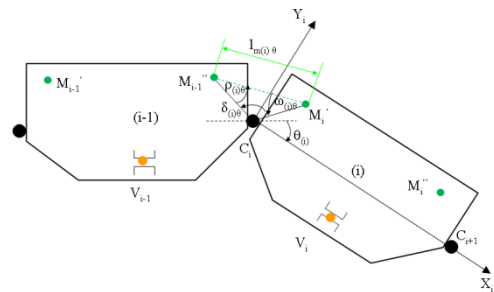


Figure 13. Elastic element diagram for two contiguous phalanges with $\theta_i > 0$

As for the tendon, in this case, the elongation of the spring relative to the phalanges (i-1) and (i) will be obtained from the difference between the quantities, as well as according to the relation:

$$\Delta lm_{(i)\theta} = lm_{(i)\theta} - lm_{(i)0} \quad (30)$$

4.2 Dynamic study

Considering the structure of the finger, for the dynamic study of the mechanism we will refer to the convention of "Denavit and Hartenberg" for the arrangement of the reference systems associated with each phalanx.

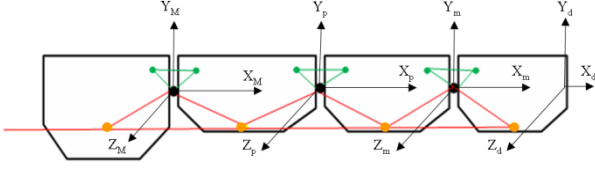


Figure 14. The “Denavit and Hartenberg” representation of the finger model

In Figure 14 the adopted arrangement of the reference systems is represented, and the subscripts “M”, “p”, “m”, “d” identify the four sets of references integral to the metacarpal, the proximal phalanx, the medial phalanx and the distal phalanx, respectively.

As is well-known, by using the Convention of “Denavit and Hartenberg” it is possible to identify the homogeneous transformation matrices that describe the relationships between the different parts of the mechanical structure that are in relative motion.

In particular, for two phalanges (i-1) and (i), the matrix ${}^{i-1}A_i$ defines the transformation between the two reference systems, (i-1) and (i), integral to the phalanges. In this way, the relationships between the distal phalanx and the metacarpal are described using the following matrix:

$${}^M A_d = {}^M A_p \cdot {}^p A_m \cdot {}^m A_d \quad (31)$$

4.2.1 Dynamic equilibrium of the phalanx

The dynamic equilibrium of any of the phalanxes was modelled as suggested in [17] for a generic multi-link system.

Figure 15 shows the generic phalanx; to analyse its dynamic equilibrium we must consider the following actions:

- $[\Phi_i]^{(e)}$ = actions of external forces applied to the phalanx (i) including those of the forces of inertia and of gravitational force;
- $[\Phi_i]$ = actions that the phalanx (i) exercise on the (i-1), including reaction forces
- $[\Phi_{i+1}]$ = actions that the phalanx (i+1) exercise on the phalanx (i).

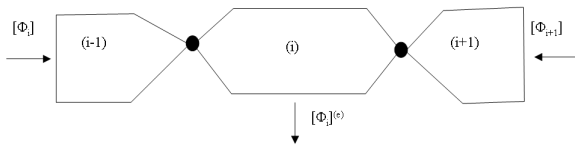


Figure 15. Actions on the phalanx (i)

The dynamic equilibrium is expressed by the following relationship:

$$\begin{aligned} -[\Phi_i] + [\Phi_i]^{(e)} + [\Phi_{i+1}] &= [0] \\ \Downarrow \\ [\Phi_i] &= [\Phi_i]^{(e)} + [\Phi_{i+1}] \end{aligned} \quad (32)$$

In particular, the action $[\Phi_i]^{(e)}$ can be expressed as:

$$\begin{aligned} [\Phi_i]^{(e)} &= -[{}^0 W_i][Y_i] + [Y_i][{}^0 W_i]^T + \\ &+ [W_g][Y_i] - [Y_i][W_g]^T + [\Phi^*] \end{aligned} \quad (33)$$

In the previous relation:

${}^0 W_i$ is the absolute acceleration matrix of the phalanx (i) with respect to an inertial reference (0), projected on the reference integral to the phalanx (i);

$[Y_i]$ is an inertia matrix (pseudo-tensor of inertia) that takes into account the mass distribution of the phalanx with respect to the reference system (i), integral to the phalanx;

$[W_g]$ is the matrix of the gravity acceleration;

$[\Phi^*]$ is the matrix that takes into account other external forces.

5. Simulation results of the finger model

Starting from an initial undeformed configuration, in which the tendon is of a certain length, if three rotations of the phalanges are assigned, the tendon is shortened by an amount that depends on the imposed rotations, from the positions of the pulleys and hinges and by the characteristics of the elements' elasticity.

If the possible configurations of the finger need to be controlled by a single actuator, due to the adaptive system described above, it is not sufficient simply to assign the shortening of the tendon. The mechanism, in fact, assumes a different configuration depending on the stiffness of the elastic elements. With the aim of studying a mechanism, the kinematics of which can be fully controlled by a single actuator, a model of the articulated finger was developed using a piece of simulation software. In particular, a data flow graphical programming language tool was used for modelling, simulating and analysing multi-domain dynamic systems.

The development of the model can be divided into three different phases. In the first step, the mechanical structure was reproduced simply by means of preset blocks to simulate the bodies, hinges and springs. In the second phase the model of the tendon was studied, introducing geometric relationships to the model that allow it to compute the components of the forces that the tendon applies to the system through the pulleys. The third phase involved the development of strategies for controlling the pulling force and the stiffness of the elastic elements, to obtain the desired configuration of the entire structure.

The mechanical structure was completely modelled using four preset fundamental blocks:

- The “Body” block for modelling the phalanges and the metacarpal;
- The “Revolute” block for modelling the hinges of the knuckles;

- The "Weld" block for modelling the metacarpophalangeal joint;
- The "Body Spring & Damper" block for modelling the elastic elements' actions.

For each block, "Revolute" is associated with an action of "hard stop" to impose a limit on the maximum guaranteed rotation, thus simulating a mechanical stop in both directions.

In Figure 16 a graphical representation of the model of the finger is shown.

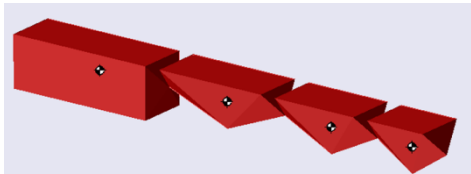


Figure 16. Finger model

The simulation of the tendon and the pulleys on which it moves, is set by calculating the forces that the pulleys transmit on the structure due to the pulling force of the tendon, as is shown in Figure 17. From this schematic, it is also possible to evaluate the local shortening of the tendon 18) relative to each phalanx and the total shortening relative to the entire finger 19).

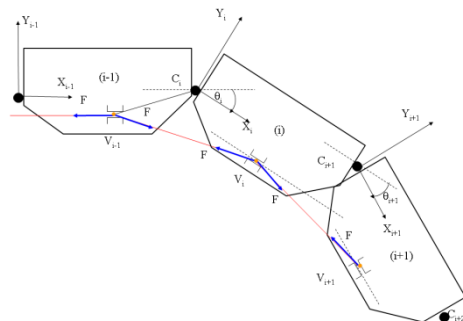


Figure 17. Tendon action

By using equations 9, 14 and 15, the components of the pulling force can be computed; then these components are applied at the point where the pulley is positioned, while the local instantaneous shortening of the tendon is sent to the control system.

The finger configuration is controlled by using four separate controllers. One is applied to the traction force controlling the total shortening of the tendon, the other three are applied to the stiffness of the elastic elements positioned on the knuckles, controlling the three individual rotations of the phalanges.

The first simulation was performed by considering a system in which the traction force of the tendon is

controlled and the stiffness of the elastic elements is constant. The finger is thus operated by a variable and controlled traction force, and the stiffness of the elastic elements of the knuckles is constant.

In Table 2, one set of simulation parameters is shown.

	Phalanx		
	Proximal	Middle	Distal
Rotation (θ_i)	5°	10°	15°
Stiffness (K_i)	15000 N/m	5000 N/m	1100 N/m

Table 2. Simulation parameters

In Figure 18 some results are shown.

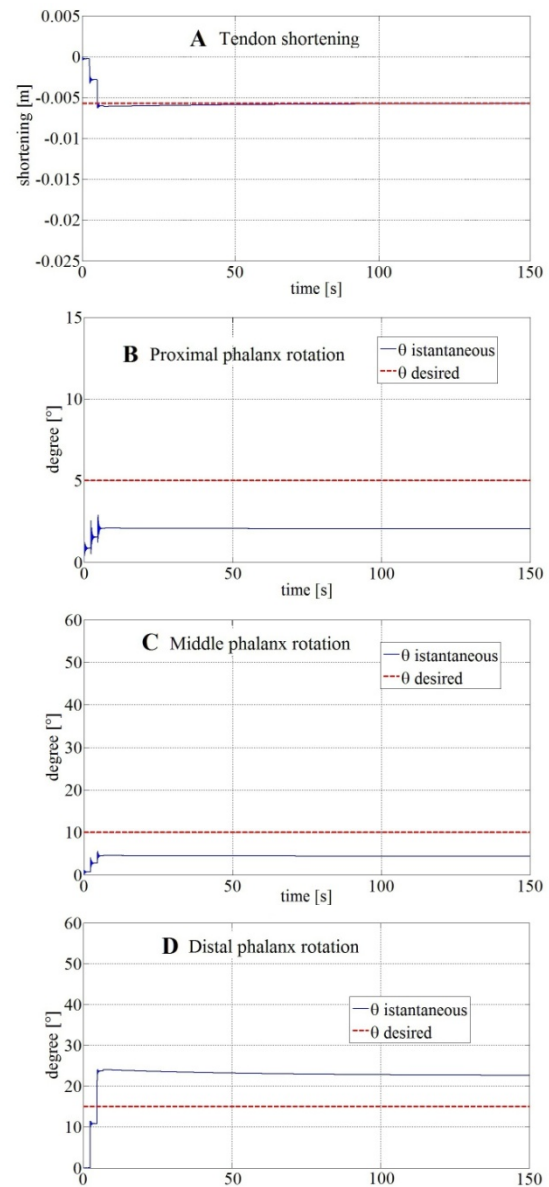


Figure 18. Simulation results with controlled traction force and constant stiffness

The simulation results show that the control system for force works properly since the tendon actually reaches the desired shortening, obtained on the basis of the established rotations of the phalanges, but they also highlight the impossibility of obtaining any configuration by assigning and controlling only the quantity by which the tendon should be shortened. Figure 18-A shows how the force control system should operate, with the total shortening of the tendon reaching the desired value. Figures 18-B, 18-C and 18-D show the evolution of the rotations of the phalanges, which are all far from the desired values. Therefore, assigning a set of constant stiffnesses and a certain shortening of the tendon, an articulated mechanism of this type assumes the existence of a configuration that is very precise which depends also on the stiffness values.

In the second type of simulation, the finger is operated by a constant traction force, and the stiffness of the elastic elements of the knuckles are variable and controlled. The set of starting values of the stiffness and the three required rotations of the phalanges are the same as shown in Table 2.

In Figure 19-A, 19-B, 19-C and 19-D the simulation results obtained with a traction force of 15N are shown. By varying the stiffness in order to control the three required rotations of the phalanges, the system achieves the desired configuration.

In Figure 20-A, 20-B, 20-C and 20-D the simulation results obtained with a traction force of 10N are shown.

By comparing the results obtained with the two different traction forces, it can be observed that the main difference concerns the duration of the transitory, which, in the case of a traction force of 10N, appears to be shorter. This means that for each desired configuration there is an ideal value for the force which allows the system to respond in an optimal manner, but also means that by repeating the simulation with lower values of traction force there are cases in which the system fails to achieve the desired configuration.

In the third simulation, the finger is operated by a variable and controlled traction force, and the stiffness of elastic elements of the knuckles are variable and controlled. The simulation parameters are always those shown in Table 2.

The simulation results show that the combined action of the two control systems is effective, even if the duration of the transitory of the law of motion of the three phalanges increases. In Figures 21-A, 21-B, 21-C and 21-D the results are shown.

The problem of the transitory duration must surely be approached by adopting more complex controllers than the simple PID used in the simulations.

However, the main advantage of having the two controls is being able to achieve any configuration simply by assigning the required rotations and delegating to the control system the assessment of the stiffness and of the force to be applied.

For each desired configuration, therefore, the system operates autonomously, changing both the stiffness and the traction force.

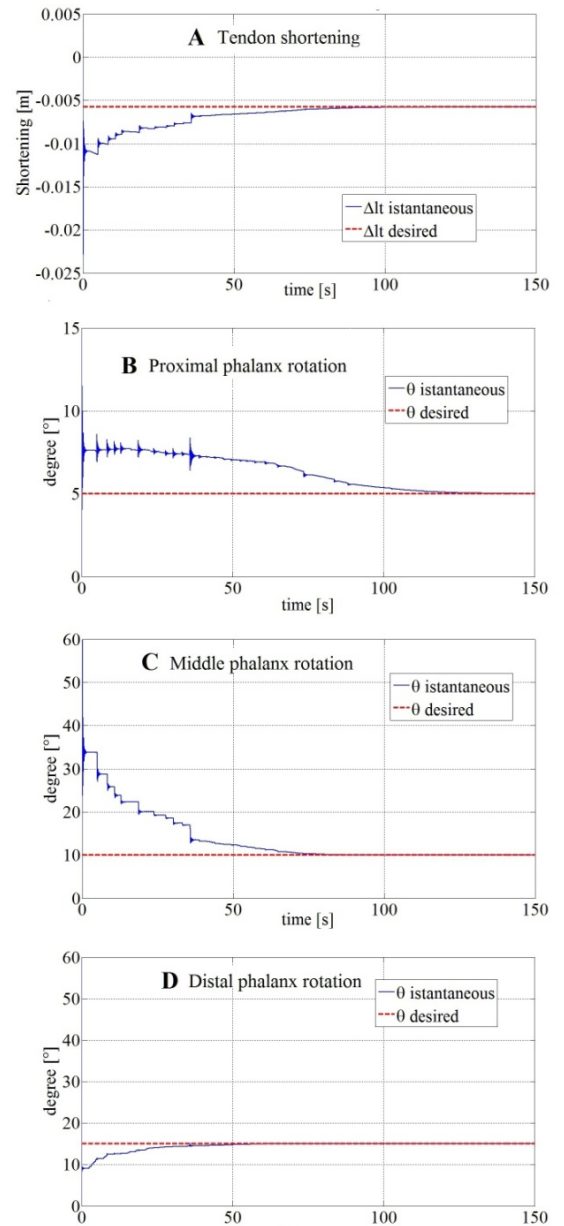


Figure 19. Simulation results with a constant traction force of 15N and controlled stiffness

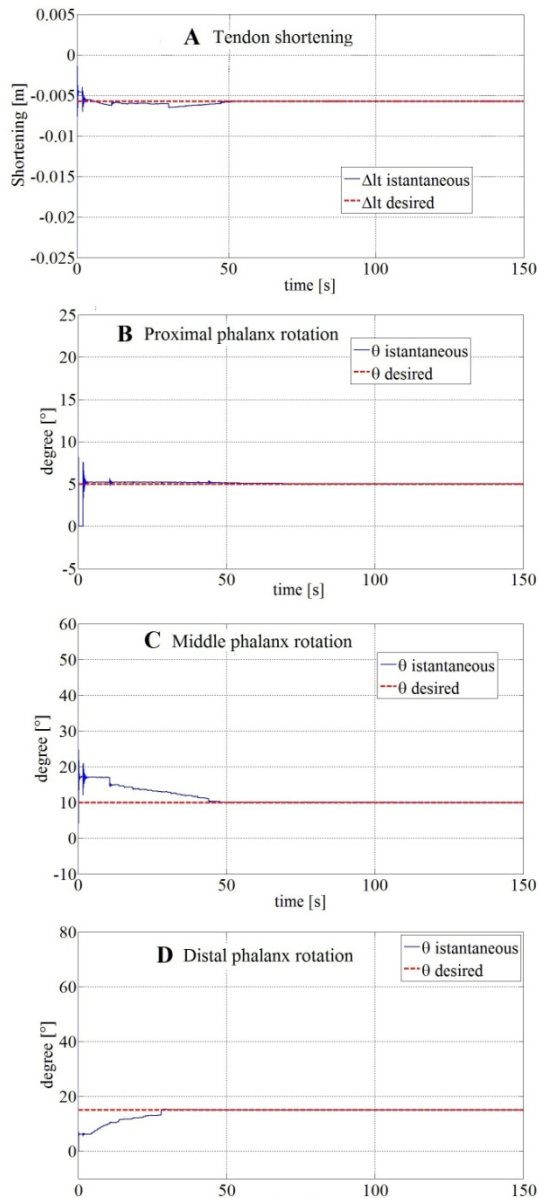


Figure 20. Simulation results with constant traction force of 10N and controlled stiffness

It must be observed that, with this double control, it is also possible to achieve different configurations of the fingers with the same applied traction force.

A simplified solution could be obtained with a locking system for each of the joints with an on/off action.

A visualization of what it happens when controlled stiffness spring are used can be observed in Figure 22. In the Figure a simulation results by Working Model 2D™ of the mechanism is reported: the actuator always exerts the same force; on the left the springs have all the same stiffness while on the right the stiffness indicated with L were significantly decreased and those indicated with I were significantly increased. The difference in the fingers configuration is evident.

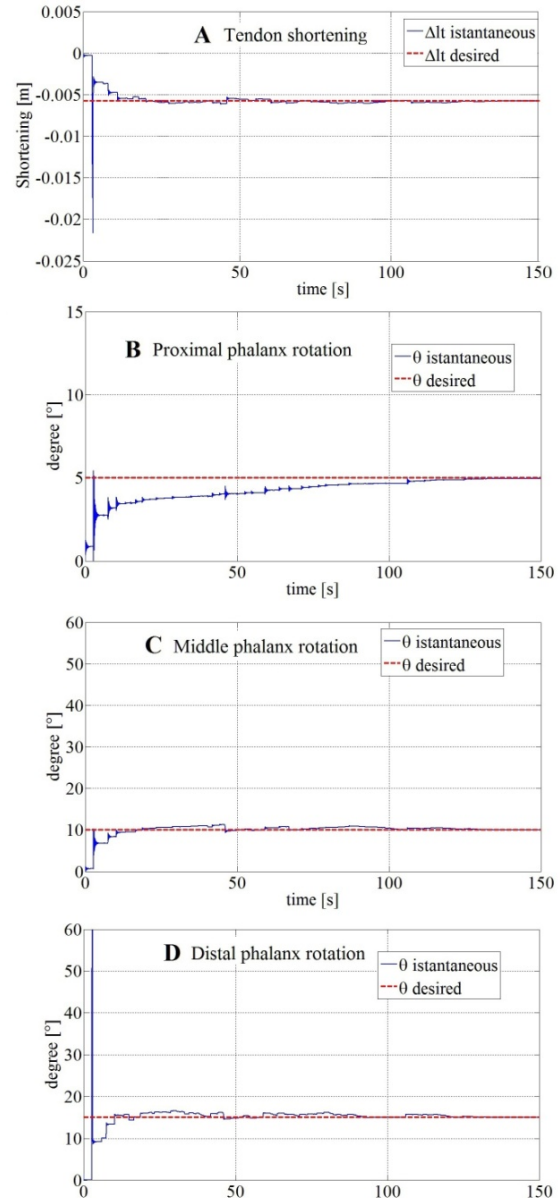


Figure 21. Simulation results with controlled traction force and controlled stiffness

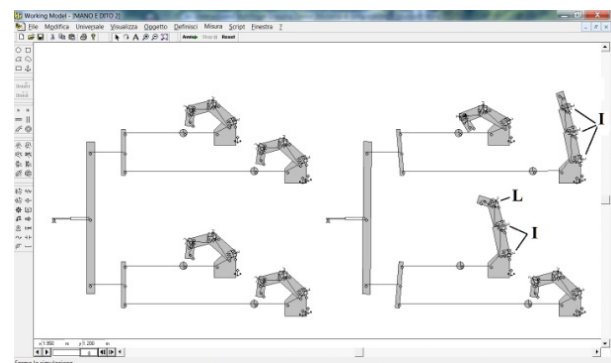


Figure 22. Simulation results from Working Model 2D™

6. Conclusions

An Underactuated Multi-finger Grasping Device was presented in this paper. The device can be used both as a robot grasping tool and as a human hand prosthesis. Both kinematic and dynamic studies were carried out on the finger mechanism and finally some test results were also presented for the finger itself as well as for the entire grasping device.

The device is adaptive since the fingers' phalanges, during the grasping motion, rotate and come into contact with the object surface for objects of almost any shape. This occurs without the need for any control system. This was clearly shown in Figure 6.

If stiffness is controlled, the simulation results show interesting possibilities and, in particular, different finger configurations than for the actuator of the same force.

Further investigations will deal with the improvements reported above. Presently, in order to improve the ability of the hand, the following possibilities were conceived.

There is the possibility of modifying the stiffness, which could be based on the use of elastic elements made with magnetorheological elastomers.

Another (simpler) technique could be to use an antagonist tendon for each finger. In this way it is not possible to control the stiffness of each phalanx, but, however, it is possible to modify the configuration of the fingers with the same traction force.

Another solution would be to provide a locking system with an on/off action at any of the joints.

7. References

- [1] Gosselin C., Pelletier F., and Laliberte T. (2008) An Anthropomorphic Underactuated Robotic Hand with 15 Dofs and a Single Actuator. 2008 IEEE Int. Conf. on Robotics and Automation Pasadena, CA, USA, May 19-23, 2008.
- [2] Brown C.Y., and Asada H.H. (2007) Inter-Finger Coordination and Postural Synergies in Robot Hands via Mechanical Implementation of Principal Components Analysis. 2007 IEEE/RSJ Int. Conf. on Intelligent Robots and Systems San Diego, CA, USA, Oct 29 - Nov 2, 2007
- [3] Grebenstein M., Chalon M., Hirzinger G., and Siegwart R. (2010) Antagonistically Driven Finger Design for the Anthropomorphic DLR Hand Arm System. IEEE-RAS International Conference on Humanoid Robots Nashville, TN, USA, December 6-8, 2010
- [4] Controzzi M., Cipriani C., and Carrozza M.C. (2008) Mechatronic Design of a Transradial Cybernetic Hand. IROS February 22, 2008
- [5] Cipriani C., Controzzi M., and Carrozza M.C. (2011) The Smart Hand Transradial Prosthesis, Journal Of Neuro-engineering And Rehabilitation, 2011, n. 8.
- [6] Roccella S., Carrozza M.C., Cappiello G., Dario P., Cabibihan J.J., Zecca M., Miwa H., Itoh K., Matsumoto M., and Takanishi A. (2004) Design, fabrication and preliminary results of a Novel anthropomorphic hand for humanoid robotics: RCH-1, Proceedings of 2004 IEEE/RSJ International Conference on Intelligent Robots and Systems, Sendai, Japan, September 28 - October 2, 2004.
- [7] Roccella S., Carrozza M.C., Cappiello G., Cabibihan J.J., Laschi C., Dario P., Takanobu H., Matsumoto M., Miwa H., Itoh K., Takanishi A. (2007) Design and Development of Five-Fingered Hands for a Humanoid Emotion Expression Robot, International Journal Of Humanoid Robotics, 2007, n. 4, pp. 181-206.
- [8] Roccella S., Cattin E., Vitiello N., Giovacchini F., Chiri A., Vecchi F., Carrozza M.C. (2008) Design of a hand exoskeleton (handexos) for the rehabilitation of the hand, Gerontechnology; N. 7(2), 2008, pp. 197:197
- [9] Catalano M.G., Grioli G., Serio A., Farnioli E., Piazza C., Bicchi A. (2012) Adaptive Synergies for a Humanoid Robot Hand. Proc. of IEEE-RAS International Conference on Humanoid Robots Osaka, Japan, Nov. 29th - Dec. 1st, 2012.
- [10] Pylatiuk C., Mounier S., Kargov A., Schulz S., Bretthauer G. (2004) Progress in the Development of a Multifunctional Hand Prosthesis. Proc. of the 26th Annual International Conf. of the IEEE EMBS San Francisco, CA, USA, September 1-5, 2004
- [11] Carbone G., and Ceccarelli M. (2008) 'Experimental Tests on Feasible Operation of a Finger Mechanism in the LARM Hand ', Mechanics Based Design of Structures and Machines, 36:1, 1 - 13 DOI: 10.1080/15397730701729445
- [12] Cheng W.L., Carbone G., and Ceccarelli M. (2009) 'Designing an underactuated mechanism for a 1 active DOF finger operation' Mechanism and Machine Theory 44 (2009) 336-348
- [13] Carbone G., and Ceccarelli M. (2008) 'Design of LARM Hand: Problems and Solutions' Journal of Control Engineering and Applied Informatics, Vol.10, n.2, pp. 39-46.
- [14] Yao S., Ceccarelli M., Carbone G., Zhan Q., and Lu Z. (2011) 'Analysis and optimal design of an underactuated finger mechanism for LARM hand' Front. Mech. Eng. 2011, 6(3): 332-343 DOI 10.1007/s11465-011-0229-8
- [15] Cotton D.P.J., Cranny A., Chappell P.H., White N.M., and Beeby S.P. (2006) Control Strategies For A Multiple Degree Of Freedom Prosthetic Hand.

Electronic Systems Design Group, School of Electronics and Computer Science, University of Southampton, 2006

- [16] Baril M., Laliberte T., Gosselin C., and Routhier F. (2013) On the Design of a Mechanically Programmable Underactuated Anthropomorphic Prosthetic Gripper. *J. Mech. Des.* 135(12), 121008 doi:10.1115/1.4025493
- [17] Lotti F., Vassura G. (2012) Sviluppo Di Soluzioni Innovative Per La Struttura Meccanica Di Dita Articolate Per Mani Robotiche. Associazione Italiana per l'Analisi delle Sollecitazioni (AIAS) XXXI Convegno Nazionale, 18-21 Settembre 2002, Parma.